Materials Science-Poland, 41(2), 2023, pp. 383-400
http://www.materialsscience.pwr.wroc.pl/
DOI: 10.2478/msp-2023-0023

Investigation of additive manufactured micro-lattice structures for defence applications

Ameer Malik Shaik[1,2], Bobbili Veera Siva Reddy[2,*], C. Chandrasekhara Sastry[3,*], J. Krishnaiah[4], B. Ramakrishna[5]

[1]Scientist E, Combat Vehicle Research Establishment (CVRDE), Defence Research Development Organization (DRDO), Avadi, Chennai 600054, Tamil Nadu, Chennai

[2]Research Scholar, Department of Mechanical Engineering, Indian Institute of Information Technology Design and Manufacturing Kurnool (IIITDMK), 518008, Andhra Pradesh, India

[3]Assistant Professor, Department of Mechanical Engineering, Indian Institute of Information Technology Design and Manufacturing Kurnool (IIITDMK), 518008, Andhra Pradesh, India

[4]Associate Professor, Department of Mechanical Engineering, Indian Institute of Information Technology Design and Manufacturing Kurnool (IIITDMK), 518008, Andhra Pradesh, India

[5]Scientist G, Defence Metallurgical Research Laboratory (DMRL), Hyderabad 500066, Telangana, India

This study investigates the blast mitigation capabilities of A286 steel micro-lattice structures produced through additive manufacturing. The research explores the effects of different manufacturing conditions, such as stress relief and heat treatment, on the mechanical properties and blast resistance of honeycomb and gyroid lattice structures in correlation with armour steel structures. Comprehensive evaluations, including surface morphology, corrosion resistance, and compressive residual stress analysis, reveal notable findings for micro-lattice structures. Micro-lattice structures demonstrated 57.23% higher corrosion resistance compared to conventional materials, presently available in the form of rolled homogeneous armour, medium hardness armour, and high-nitrogen steel. Additionally, honeycomb lattice structures exhibit compressive residual stresses of up to 581.90 MPa, providing significant advantages in blast mitigation potential. These results underscore the significance of lattice geometry, material microstructure, and residual stress in enhancing blast resistance. The research offers valuable insights into optimizing additive manufactured structures as an alternative modular solution for defence applications.

Keywords: *additive manufacturing, corrosion, hardness, micro-lattice, morphology, residual stress*

1. Introduction

The demand for sandwich structures in the aerospace, automotive, marine, and defence industries has sparked research into optimizing core materials for better energy absorption in crash performance [1]. Traditional cellular materials like honeycomb [2] and foam have advantages in stiffness and energy dissipation but face drawbacks of high manufacturing costs and moisture retention. Micro-lattice materials, produced using 3D printing, offer intricate structures with impressive strength-to-weight ratios, providing potential solutions to these drawbacks.

In defence applications, 3D-printed micro-lattice structures hold promise for blast mitigation due to their high porosity, enabling efficient energy absorption and dissipation [3, 4]. When exposed to impact or blast, these structures buckle or fracture individual struts while preserving overall integrity [5]. Such traits make them ideal for protective gear, building designs in high-risk areas, and in the aerospace and defence industries, especially in the area of armoured fighting vehicles (AFVs).

As the AFVs are subjected to disparate terrains, corrosion is a natural and often destructive process that affects metallic materials over time,

* E-mail: sivareddy.bobbili@gmail.com; chandrasekhar@iiitk.ac.in

© Ameer Malik Shaik et al. 2023. This is an open access article distributed under the Creative Commons Attribution-NonCommercial-NoDerivatives 4.0 License. (http://creativecommons.org/licenses/by-nc-nd/4.0/)

and with major impact in the underbody parts, thus reducing strength on an exponential scale. Corrosion involves the deterioration of a material due to chemical reactions with its environment. This phenomenon can weaken materials, compromise their structural integrity, and reduce their longevity [6, 7]. In aerospace and defence engineering, corrosion is a critical concern, particularly when dealing with materials intended for harsh or challenging environments. Effective strategies for preventing or mitigating corrosion are essential for maintaining the reliability and safety of various structures and systems, which is yet to be explored for micro-lattice structures, as construction of the underbody structures to this date are limited only to the various conventional grades of steel.

Residual stress is a state of internal stress that remains within a material even after all external forces are removed. It can arise during certain manufacturing processes, including welding, heat treatment, and additive manufacturing (3D printing) [8]. Residual stress can have significant implications for a material's properties and performance. Understanding and managing residual stresses are crucial, especially in applications where mechanical integrity and durability are paramount, especially in the context of AFVs. In industries such as aerospace, automotive, and defence, where materials are exposed to extreme conditions, analysing and optimising residual stress become critical for ensuring the reliability and safety of components.

For armoured fighting vehicles (AFVs), 3D-printed micro-lattice materials [9] should be explored for efficient blast mitigation without the weight and volume penalties associated with the traditional methods like V-shaped floors and metallic foams. These materials provide high energy absorption with reduced space constraints, making them a promising alternative for enhancing AFV survivability [10]. In this regard, therefore, our research aims to provide a modular solution, in order to reduce the weight factor without compromising on the metallurgical and blast mitigation capabilities of the AFVs. For this purpose, development of metallic micro-lattice honeycomb and gyroid structures is done using A286 steel through the laser powder bed fusion (LPBF) process, with appropriate design incorporations as per defence requirements. The A286 steel analysed corresponds to the ISO label 'ISO 630-6:2014', previously in the standard of ISO 24314:2006 (high-load structural steel), and the test coupons fastened to the AFVs underbelly, are ISO 3506. This ISO label represents the A286 steel alloy, which is a heat- and corrosion-resistant alloy widely used in high-temperature applications. These metallic micro-additive structures are developed as test specimens and evaluated in correlation to armoured steel. An optimal process window is obtained to optimise strength with minimal porosity and anisotropy for micro-lattice structures and further correlating scientific comparison with conventional armour materials that are currently used in AFVs, which are sourced from main battle tanks from defence research labs (CVRDE and DMRL) to ensure that a one-to-one correlation is met, and also that the enhanced capabilities of the microstructure are presented.

2. Materials and methods

2.1. Present material: defence application

Three types of steel used in defence applications for AFVs are rolled homogeneous armour (RHA), modified homogeneous armour (MHA), and high non-magnetic steel (HNS). RHA is a standard high-strength low alloy steel with a tensile strength of 900–1050 MPa and a hardness of around 300 VHN. MHA, an stainless steel, offers improved ballistic protection with a tensile strength of 1300–1450 MPa and a hardness of about 450 VHN. HNS is designed for special grade armour applications, boasting a tensile strength of 940–1075 MPa and a hardness of approximately 270 VHN. HNS is used particularly in AFV floor plates due to its nonmagnetic nature and cost-effectiveness, being 30% to 40% cheaper than RHA. The integration of these materials into AFVs, however, results in weight, manoeuvrability, and stability issues. Researchers are exploring micro-lattice structures, for which we propose honeycomb and gyroid, additively

Table 1. Micro-lattice structure design variations

Gyroid	**Design 1**				
Dimensions (L × W × H) (mm)	24 × 20 × 30				
Honeycomb	**Design 1**	**Design 2**	**Design 3**	**Design 4**	**Design 5**
Dimensions (L × W × H) (mm)	24 × 20 × 30				
Wall thickness (mm)	2	2	2	2	2
Detail size (mm)	1	1	1	1	1
Hole diameter (mm)	1.4	1.2	1	0.8	0.5
Infill thickness (mm)	1.4	1.2	1	0.8	0.5

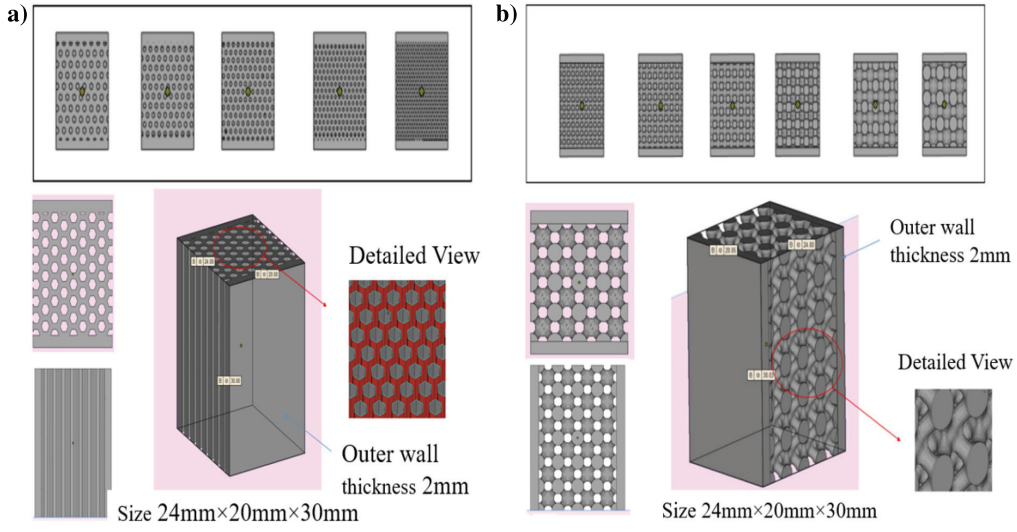


Fig. 1. Micro-lattice structure design: (a) honeycomb and (b) gyroid

manufactured by laser powder bed fusion (LPBF) to address these concerns and reduce weight and thickness without compromising mechanical properties and blast mitigation capabilities.

2.2. Micro-lattice design module

The honeycomb and gyroid test specimens' final designs are achieved through collaboration with defence research labs (CVRDE and DMRL) and an end-to-end study. Table 1 showcases the designs obtained after multiple trial-and-error iterations. Figure 1 illustrates the individual designs of the honeycomb and gyroid structures to ensure optimal weight reduction is achieved without compromising integrity elements. The design iteration follows a similar approach to the sandwich panel, incorporating a 2-mm outer thickness to meet the testing requirements and facilitate attachment to AFV underbody structures.

2.3. Micro-lattice printing by LPBF process

2.3.1. Raw material – A286 powder

For development of micro-lattice structures, A286 powder is used for metallic printing of test specimens, due to its high-strength capability, paired with corrosion resistance, which are eternal requirements of AFV underbody modules. The resulting powder specimens were subjected to a thorough morphological analysis, and also ensuring post-machining capability and hardness over nickel/cobalt steels, makes it durable product citing its capacity of use. The physical and chemical properties are presented in Table 2; testing on 10 samples was performed in Omega Inspection and Analytical Laboratory, Chennai, Tamil Nadu, India, to determine the mechanical and metallurgical properties. The elemental composition was

Table 2. Physical properties of A286 steel

Property	**Value**
Ultimate tensile strength	620 MPa
Yield strength	275 MPa
Elongation at break	40%
Modulus of elasticity	201 GPa
Poisson's ratio	0.3
Shear modulus	77 GPa
Reduction of area	20%

Chemical composition (% weight factor) of A286 steel													
Element	**C**	**Mn**	**Si**	**P**	**S**	**Ni**	**Cr**	**Mo**	**V**	**Al**	**Ti**	**Cu**	**Fe**
Weight (%)	0.034	0.126	0.236	0.012	0.006	25.62	15.40	1.331	0.196	0.209	2.054	0.014	Bal.

Table 3. Particle size distribution – sieve analysis

Particle size (μm)	**Sieve number**	**% by mass**
<45	−325	78.28
>45	+325	17.28
>53	+270	3.78
>63	+230	0.65

Table 4. Flow rate, apparent, and tap density test results

Test	**Test method**	**Results**
Flow rate	ASTM B213	18s/50g
Apparent density	ASTM B212	3.98g/cm^3
Tap density	ASTM B527	4.65g/cm^3

further tested in Wipro 3D, before metal printing to substantiate the process.

2.3.2. Particle size

The analysis of particle size distribution was conducted in accordance with the ASTM B214 standard, and the outcomes have been presented in Table 3.

2.3.3. Flowability, apparent and tap density

Table 4 presents the results of flow rate, apparent density, and tap density tests conducted on HRS-A286 metal powder. The table includes information on the test methods and the corresponding results for each test.

2.3.4. LPBF process

The printing of the A286 steel micro-lattice specimens was carried out on an EOS M290 LPBF machine as shown in Figure 2a. The test specimens with integrated lattice structures were built using vacuum inert gas atomized powders of A286 steel; the laser source used in the LPBF machine was a discontinuous Yb-Fiber laser of 1000 W, with a maximum power at a laser beam diameter of 75 μm. The build volume was $250 \times 250 \times 325\,\text{mm}^3$, and the powder layer's thickness during the building was set at 20 μm. The manufactured specimens are shown in Figure 2b. The parts are separated from the bottom supporting plate by wire electric discharge machining (w-EDM) shown in Figure 2c.

2.3.5. Post-process treatment of micro-lattice specimens

Lattice structure coupon parts were stress-relieved following AMS 2773 with solution treatment and precipitation hardening. Solution treatment was carried out between 900°C and 1100°C for 60 minutes and oil quenched. Furthermore, precipitation hardening was carried out between 680°C and 750°C for 16 hours and air-cooled. This process was used to ensure reduction of residual stresses, enhance structural integrity, and additionally optimize the lattice microstructure. This results in superior strength, toughness, and blast resistance, and makes the parts highly effective for AFVs and in industries requiring safety and protection against stress and blast loads.

2.4. Experimental evaluation for the LPBF process

Designing armour for the AFV66 as a parameter for evaluation for the design module specimens

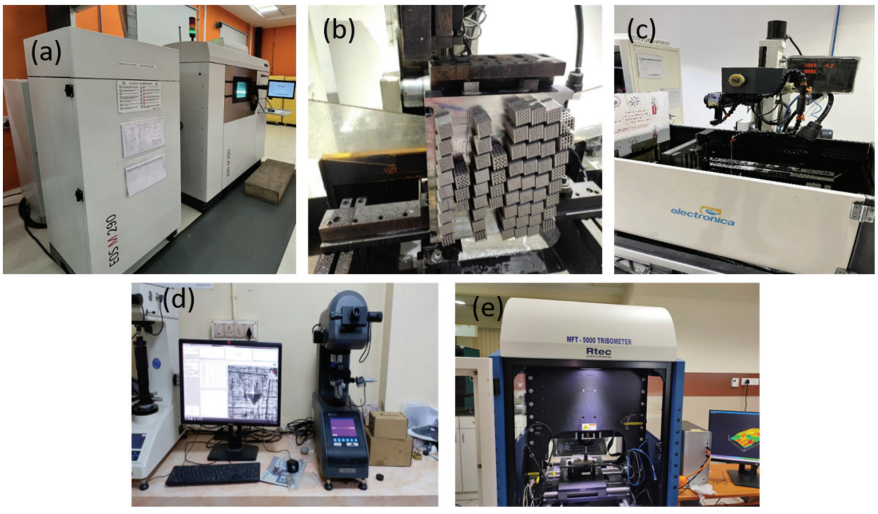


Fig. 2. (a) Laser powder bed fusion process for printing of micro-lattice specimens: EOS M290; (b) micro-lattice specimens honeycomb and gyroid; (c) w-EDM machine; (d) Micro Vickers hardness machine; (e) surface roughness measurement device

against explosive attacks requires considering surface roughness and micro-Vickers hardness. Surface roughness impacts blast loading performance, while micro-Vickers hardness determines strength and resistance to deformation. LPBF-manufactured specimens undergo analysis for different conditions to enhance protection [11]. The microhardness of the micro-lattice structure test specimen was carried out as per the ISO 14577-1 standard, using Tukon/Wilson 1102 - Vickers (scale: microns) illustrated in Figure 2d, with dead weight loads of 0.01 to 1-kg and 2-kg options. The number of measurements were six per sample in order to obtain average values on the same surface after multiple indentations owing to the intricate features of the lattice structures. In the roughness measurement process, a total of four different locations on the front view of the lattice structure were selected for measurement. The measurements were taken using the MFT-5000 Tribometer (RTEC Instruments) with an R-20x lens and white light as indicated in Figure 2e. The software Gwyddion (64 bit) was employed for post-processing of the acquired data. The measurements were conducted to assess the surface roughness of the lattice structures. These measurements provided insights into the average surface roughness values at the specified locations, contributing to our understanding of the surface quality and characteristics of the lattice structures.

The objective of this investigation is to improve the protective capacity of the armour against explosive attacks. Tables 5 and 6 present the response variables related to the design criteria for honeycomb and gyroid micro-lattice structures, respectively. The gyroid is a surface of minimal dimensions featuring a profoundly intricate geometric structure that presents a repetitive arrangement of interlinked struts, thereby limiting consideration to only one type of design. It is distinguished by its elaborate and sponge-like visual aesthetics. As a result of the high volume of specimens, unique codes have been assigned to each one. The specimens were divided equally into 'As Printed' or 'Non-Stress Relieved' (designated as 'A'), 'Stress Relieved' (designated as 'B'), and the final 'Heat Treated' (designated as 'C', 'D', and 'E'). Specimens were distributed in sets of three to facilitate diverse analyses. The six specimens of each section were further subdivided into structures of gyroid or honeycomb.

The two parameters under consideration were surface roughness and micro-Vickers hardness. The desired output was minimal surface roughness and maximum micro-Vickers hardness. These parameters are preferred, as they lead to a reduction

Table 5. Response variables, surface roughness, and micro-Vickers hardness for the honeycomb micro-lattice structure

Non-stress relived (as printed)									
				Surface roughness (Ra)			**Micro-Vickers Hardness (HV)**		
S. No.	**Lattice**	**Design**	**Non-stress relieved**	**Average (Ra)**	**Max**	**Min**	**Average**	**Max**	**Min**
1	Honeycomb	Design 1	2A	11.29	11.64	10.54	219HV1	225	213
2	Honeycomb	Design 2	3A	9.94	11.84	9.36	220HV1	227	215
3	Honeycomb	Design 3	4A	11.18	11.18	9.87	230HV1	242	218
4	Honeycomb	Design 4	5A	8.91	12.6	8.54	213HV1	218	207
5	Honeycomb	Design 5	6A	11.69	12.34	9.03	194HV1	201	190
Stress relieved									
S. No.	**Lattice**	**Design**	**Stress relieved**	**Average (Ra)**	**Max**	**Min**	**Average**	**Max**	**Min**
1	Honeycomb	Design 1	2B	14.58	24.26	9.23	233HV1	239	228
2	Honeycomb	Design 2	3B	14.79	17.12	10.48	214HV1	220	209
3	Honeycomb	Design 3	4B	13.76	15.91	12.11	193HV1	197	190
4	Honeycomb	Design 4	5B	12.26	13.66	11.43	222HV1	226	218
5	Honeycomb	Design 5	6B	20.24	24.23	17.19	220HV1	226	216
Heat treated (Final specimens)									
S. No.	**Lattice**	**Design**	**Heat treated**	**Average (Ra)**	**Max**	**Min**	**Average**	**Max**	**Min**
1	Honeycomb	Design 1	2C,2D,2E	11.59	15.2	9.12	460HV1	475	451
2	Honeycomb	Design 2	3C,3D.3E	7.77	7.94	7.65	418HV1	425	412
3	Honeycomb	Design 3	4C,4D,4E	7.67	8.46	6.63	423HV1	426	420
4	Honeycomb	Design 4	5C,5D,5E	8.82	8.87	8.77	460HV1	470	451
5	Honeycomb	Design 5	6C.6D,6E	11.92	12.81	10.41	455HV1	461	450

Table 6. Response variables, surface roughness, and micro-Vickers hardness for the gyroid micro-lattice structure

Non-stress relived (as printed)									
				Surface roughness (Ra)			**Micro-Vickers hardness (HV)**		
S. No.	**Lattice**	**Design**	**Non-Stress relieved**	**Average (Ra)**	**Max**	**Min**	**Average**	**Max**	**Min**
1	Gyroid	Design 1	1A	10.5	12.86	8.11	215HV1	220	211
Stress relieved									
S. No.	**Lattice**	**Design**	**Stress Relieved**	**Average (Ra)**	**Max**	**Min**	**Average**	**Max**	**Min**
1	Gyroid	Design 1	1B	11.85	13.46	10.83	226HV1	229	222
Heat treated (final specimens)									
S. No.	**Lattice**	**Design**	**Heat treated**	**Average (Ra)**	**Max**	**Min**	**Average**	**Max**	**Min**
1	Gyroid	Design 1	1C,1D,1E	3.56	3.74	3.37	418HV1	425	411

in localised stress concentrations and improved resistance against deformation and penetration, respectively. The vector plane that meets this criterion will be deemed a suitable test coupon dimension, as it closely approximates the optimal solution for withstanding blast loading, thereby enhancing its efficacy in safeguarding both the vehicle and its occupants. A statistical approach has been employed to identify the vector plane that best meets the specified criteria.

2.4.1. The statistical method of evolution for micro-lattice structures: MCDM TOPSIS

Multi-criteria decision-making (MCDM) involves evaluating alternatives based on multiple attributes. Statistical techniques like analytic hierarchy process (AHP), technique for order of preference by similarity to ideal solution (TOPSIS), and preference ranking organisation method for enrichment evaluations (PROMETHEE) [12] are commonly used in

MCDM. TOPSIS is favoured for its simplicity, for accommodating both quantitative and qualitative criteria, and for providing a distinct ranking of alternatives. It is widely applied in material selection, design, and in the aerospace and defence industries. The method employed to determine a solution that closely approximates the ideal is a straightforward and clear process as follows:

1. Normalization of performance:
    - Normalized performance of alternative x_i on criterion c_j is determined by:

$$r_{ij} = \frac{a_{ij}}{\sqrt{\sum_{k=1}^{n} a_{kj}^2}} \tag{1}$$

2. Weight allocation:
    - Weight w_j allocated to criterion c_j, where $w_j \geq 0$ and $\sum_{j=1}^{m} w_j = 1$.
3. Decision matrix construction:
    - Construct a matrix $R = [r_{ij}]$, where rows represent alternatives and columns represent criteria.
4. Ideal and negative ideal solutions:
    - Ideal solution $A^+ = \left(a_1^+, a_2^+, \ldots, a_m^+\right)$, where $a_j^+ = \max\left(r_{ij} \cdot w_j\right)$, where n and m are the number of rows and columns, respectively.
    - Negative ideal solution A^- is determined by $a_j^- = \min\left(r_{ij} \cdot w_j\right)$ for all alternatives $i = 1, 2, \ldots, n$.
5. Euclidean distance:
    - Distance of x_i from ideal solution:

$$S_i^+ = \sqrt{\sum_{j=1}^{m} w_j \cdot \left(r_{ij} - a_j^+\right)^2} \tag{2}$$

    - Distance of x_i from negative ideal solution:

$$S_i^- = \sqrt{\sum_{j=1}^{m} w_j \cdot \left(r_{ij} - a_j^-\right)^2} \tag{3}$$

6. Relative proximity:
    - Relative closeness of x_i to ideal solution:

$$C_i = \frac{S_i^-}{S_i^+ + S_i^-} \tag{4}$$

7. The alternatives should be ranked according to their proximity to the ideal solution.
    - The alternative that exhibits the greatest degree of relative closeness is deemed to be the optimal alternative.

The utilisation of a particular analytical approach has yielded a representation of the TOPSIS analysis pertaining to honeycomb structures in the absence of stress relief, with stress relief, and following heat treatment. Table 7 displays the findings.

Using the TOPSIS method, the optimal solution for the honeycomb A286 micro-lattice structures under different conditions as determined for non-stress-relieved and stress-relieved specimens, is the solution with dimensions of 24 mm × 20 mm × 30 mm (L × W × H) with a wall thickness of 2 mm, hole diameter of 0.8 mm, and infill thickness of 0.8 mm. For heat-treated (final) specimens, the dimensions are the same except for a hole diameter of 1 mm and an infill thickness of 1 mm.

Furthermore, this research involves an analysis and comparison of nearly optimal solutions with RHA, MHA, and HNS materials by examining their surface properties. To examine micro-lattice structures effectively, the process begins with the creation of small specimen samples that represent these intricate structures. These specimens are then cut into precise sections using wire-electrical discharge machining (W-EDM) to ensure accuracy. Each of the samples are further subjected to stress relieving and heat treatment. Any subsequent thermal residual stress caused due to W-EDM, would be compensated for in the final specimen, thereby displaying the true nature of the lattice structures. Subsequently, each specimen was meticulously ground and polished for morphological characterization, a crucial step for accurate X-ray diffraction (XRD) analysis. To eliminate any

Table 7. TOPSIS analysis for honeycomb micro-lattice structure for LPBF-generated specimens

Non-stress-relieved condition								
Normalized residual matrix			**Weighted residual matrix**		**Distance to ideal**			
Coupon no.	**NRa**	**NVHN**	**WRa**	**WVHN**	**Si+**	**Si-**	**Ci**	**Rank**
2A	0.369	0.419	0.185	0.209	0.039	0.007	0.154	4
3A	0.325	0.421	0.163	0.210	0.017	0.029	0.633	2
4A	0.365	0.440	0.183	0.220	0.037	0.010	0.204	3
5A	0.291	0.408	0.146	0.204	0.000	0.046	0.994	1
6A	0.382	0.371	0.191	0.186	0.047	0.001	0.002	5
Stress-relieved condition								
Normalized residual matrix			**Weighted residual matrix**		**Distance to ideal**			
Coupon no.	**NRa**	**NVHN**	**WRa**	**WVHN**	**Si+**	**Si-**	**Ci**	**Rank**
2B	0.477	0.446	0.239	0.223	0.038	0.094	0.713	3
3B	0.484	0.409	0.242	0.205	0.042	0.090	0.682	4
4B	0.450	0.369	0.225	0.185	0.026	0.106	0.803	2
5B	0.401	0.425	0.201	0.212	0.000	0.131	0.999	1
6B	0.662	0.421	0.331	0.210	0.131	0.001	0.005	5
Heat-treated condition								
Normalized residual matrix			**Weighted residual matrix**		**Distance to ideal**			
Coupon no.	**NRa**	**NVHN**	**WRa**	**WVHN**	**Si+**	**Si-**	**Ci**	**Rank**
2C,2D,2E	0.379	0.880	0.190	0.440	0.064	0.007	0.099	4
3C,3D.3E	0.254	0.800	0.127	0.400	0.003	0.068	0.954	2
4C,4D,4E	0.251	0.809	0.125	0.405	0.001	0.070	0.982	1
5C,5D,5E	0.289	0.880	0.144	0.440	0.019	0.052	0.736	3
6C.6D,6E	0.390	0.871	0.195	0.435	0.070	0.001	0.018	5

contaminants, the samples undergo thorough cleaning, first with acetone, then with either methanol or ethanol. The final stage before optical microscopy (OM) or scanning electron microscopy (SEM) analysis involves immersing the samples in an etchant solution for approximately 5 min. This process reveals crucial microstructural details, making the samples ready for in-depth analysis as indicated in Figure 3. The residual stress analysis of nearly optimal solutions was conducted on honeycomb and gyroid micro-lattice structures and compared with RHA, MHA, and HNS materials.

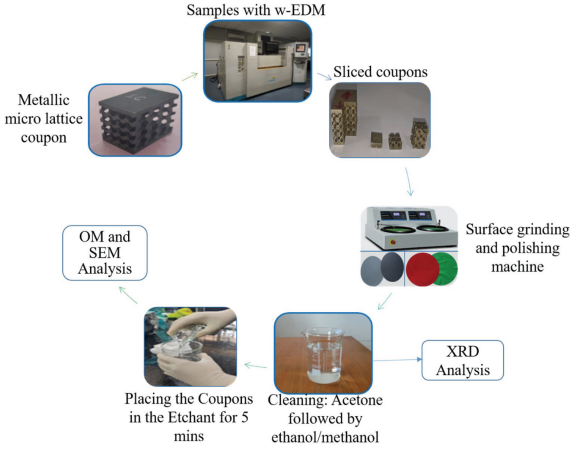


Fig. 3. Coupon preparation for morphological tests

2.5. Corrosion analysis

To evaluate corrosion resistance, accelerated laboratory corrosion tests were conducted within a controlled salt-spray chamber. This approach simulated and expedited corrosive conditions, offering insights into how well materials endure corrosion challenges. Test specimens representing various materials and structures were placed in the chamber, where a saline mist emulated harsh conditions.

Salt-spray test parameters:

- Number of specimens: For each type of structure and material, specific specimen

quantities were utilized. Honeycomb structures in both ideal and non-ideal conditions, including as-printed, stress-relieved, and heat-treated specimens, were represented by six samples each. Gyroid structures had three samples for as-printed, stress-relieved, and heat-treated conditions. Additionally, one sample each was used for RHA, MHA, and HNS materials.

- Test duration: The salt-spray tests were conducted in two cycles, each lasting 24 hours. During the first cycle, the specimens were exposed to the salt-spray chamber for 24 hours, followed by 24 hours in the atmosphere. This cycle was repeated once more for a total duration of 48 hours of exposure.
- Cleaning process: After the exposure cycles, the specimens underwent cleaning using acetone followed by methanol or ethanol to eliminate any residues or contaminants.
- Weight measurements: Weight measurements of the specimens were taken both before and after the salt-spray test cycles to assess the degree of corrosion.
- Calculation of corrosion rate: The corrosion rate was calculated based on the weight reduction of the specimens after exposure to the salt-spray environment. The corrosion rate provides a quantitative measure of the material's susceptibility to corrosion under these conditions.

These comprehensive test parameters ensure the accuracy and reliability of our corrosion analysis, allowing for a thorough assessment of corrosion resistance characteristics in the context of blast mitigation for AFVs.

2.6. Residual stress analysis

The investigation employed XRD, using a Bruker D8 XRD machine, to analyse residual stresses in studied materials, revealing insights into the internal stresses impacting mechanical properties. Evaluating residual stresses in protective structures made from RHA/MHA/HNS steels versus bulk forms must account for additive manufacturing effects. Layered printing introduces varied thermal histories and structural changes, causing distinct stress distributions. Thus, protection structures may differ from bulk materials in residual stresses due to manufacturing. Residual stress distributions significantly affect material behaviour, especially in blast mitigation. Therefore, comprehending how geometry and manufacturing impact stress patterns is vital for optimizing structural performance.

Our study focused on A286 honeycomb and gyroid micro-lattice structures fabricated via additive manufacturing. Analysing residual stress aimed to uncover links between lattice geometry, manufacturing, and stress patterns. This exploration enhances understanding of blast mitigation and structural integrity by unravelling these connections.

3. Results and discussion

3.1. Powder specimen for LPBF process: A286 steel

The powder specimens underwent examination, and the EDS assessment detailing the distribution of elements and the SEM analysis of the powdered specimen for the LPBF procedure are presented in Figure 4.

A286 steel powder exhibits exceptional properties due to the synergistic interaction of its elements. Iron provides robustness, toughness, and thermal stability, while nickel enhances high-temperature strength and ductility. Chromium improves corrosion resistance, and titanium contributes to high-temperature performance. Molybdenum enhances strength, hardness, and corrosion resistance at elevated temperatures [13]. These qualities make A286 steel powder ideal for additive manufacturing applications, including blast mitigation. Spherical powder (Figure 4d) production in LPBF ensures uniformity and efficiency in the printing process. Micro-lattice test specimens of honeycomb and gyroid structures were produced for comparison with RHA, MHA, and HNS materials, aiming to

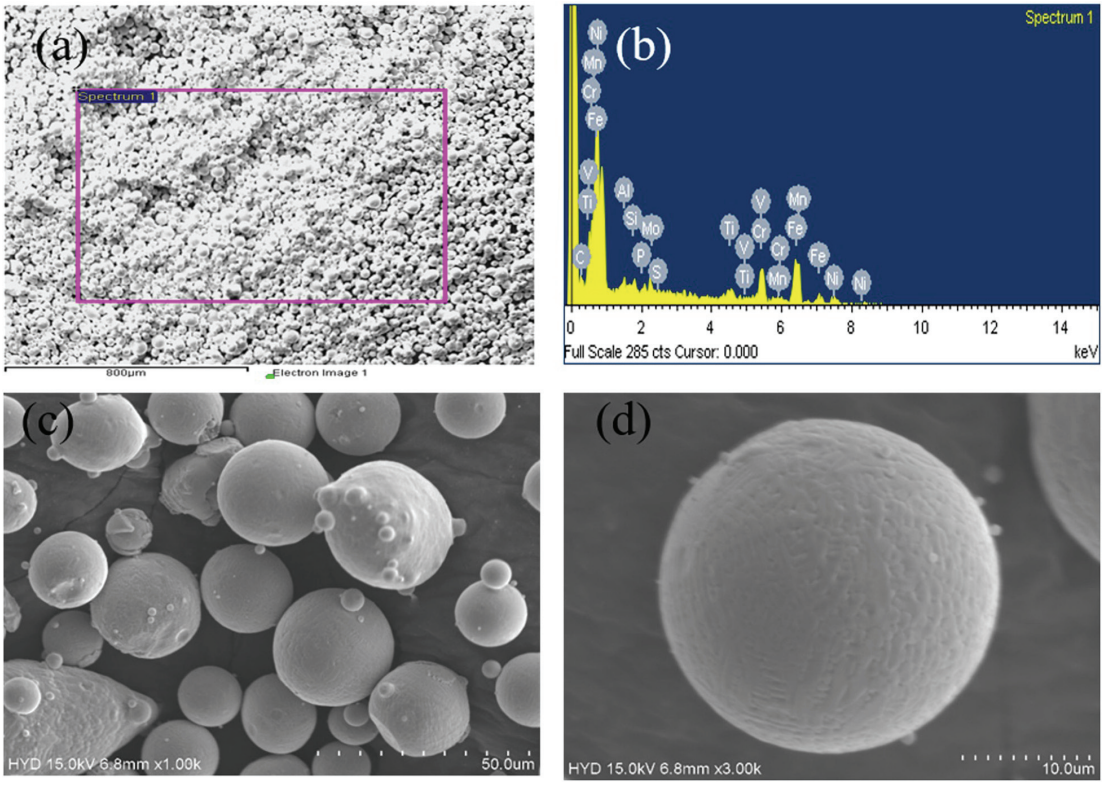


Fig. 4. LPBF A286 powder: (a) EDS analysis, (b) elemental distribution and (c, d) SEM images of A286 powder

provide an alternative underbody protection solution for AFVs.

3.2. Surface morphology

The present study investigates the correlation and comparison of A286 honeycomb and gyroid micro-lattice structures with RHA, MHA, and HNS materials. Figure 5 showcases comprehensive optical microscopy images of the RHA, MHA, and HNS materials.

Figure 5 depicts the microstructures of RHA, MHA, and HNS steels observed through OM and SEM images. Coarse grain structures in RHA steel offer advantages such as increased ductility and toughness, as well as enhanced energy absorption during explosive blasts [14], but they may act as stress concentrators leading to premature steel failure and reduced blast mitigation efficacy. Conversely, fine grain structures in MHA steel can improve strength and hardness but may increase brittleness, making it less effective in blast mitigation. HNS steel strikes a balance with its dual microstructure of fine and coarse grains. Fine grains enhance strength, toughness, and energy absorption during blasts, while coarse grains may still pose stress concentration risks with visible formation of pits present in the material. To achieve optimal blast mitigation, it is essential to optimize processing parameters and employ post-processing techniques like heat treatment, mechanical deformation, and surface treatment. These approaches can improve the microstructure of RHA, MHA, and HNS steels, enhancing their mechanical properties and overall effectiveness in minimizing the impacts of explosive blasts. Additionally, SEM images of the steel materials provide further insights. The RHA exhibits a uniform microstructure with elongated, well-defined grains, likely due to the rolling process. Surface porosity is evident, however, and can be addressed using additively manufactured A286 steel. The MHA displays a mixture of fine and coarse grains, indicating a lack of potential grain refinement processes. The HNS material

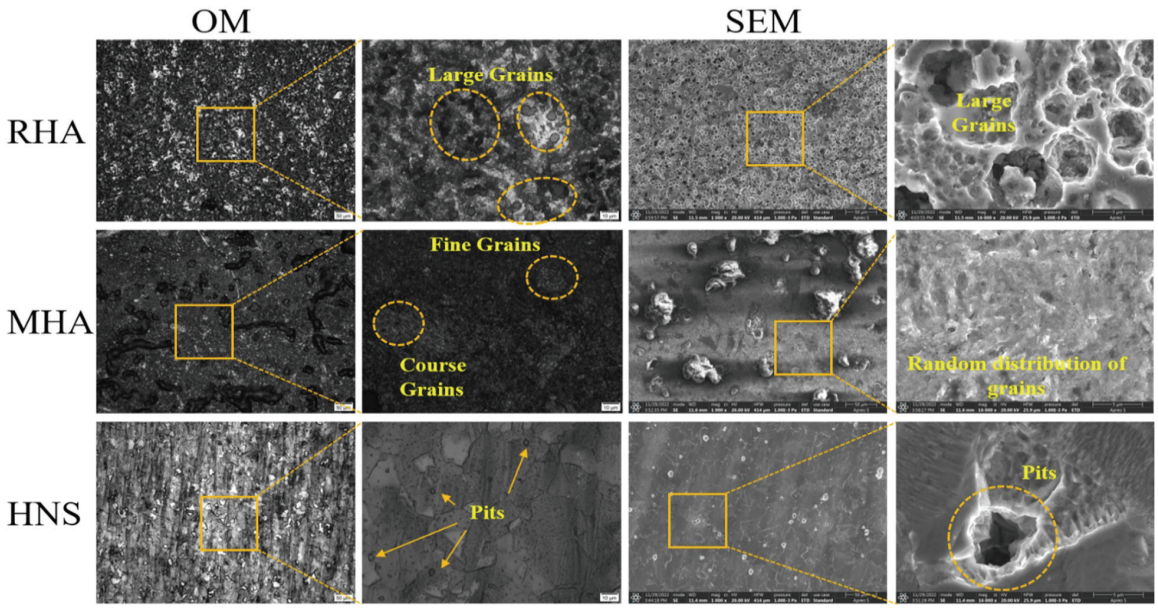


Fig. 5. OM and SEM images for (a-d) RHA (e-h) MHA (i-l) HNS

exhibits fine and coarse grains, along with additional nitrogen-containing phases that can improve mechanical and corrosion properties [15].

As a result, while the presence of both fine and coarse grains in armour steel can have an impact on its capacity to mitigate blasts, careful optimisation of the processing conditions and the use of additional post-processing techniques are needed, with a restriction of weight addition, which, for the current conventional material, results in a deadlock situation. Producing honeycomb and gyroid micro-lattice structures aids in the understanding of its evolution in blast operation as an alternative modular solution, providing an alternative for weight reduction while effectively mitigating the effects of an explosive blast [16].

Figures 6 and 7 depict OM and SEM images of honeycomb and gyroid metallic micro-lattice structures under three conditions: as-printed (non-stress relieved), stress-relieved, and heat-treated. The as-printed condition reveals voids and pores, indicating potential detrimental effects on blast mitigation capabilities. These imperfections can reduce energy absorption potential, increase vulnerability to failure upon impact, and compromise structural soundness [17]. For honeycomb structures, voids and pores compromise compression strength and energy absorption during blasts, while in gyroid structures, they can lead to stress concentration and reduced strength and stiffness. However, optimization of powder deposition parameters, inter-layer fusion, and post-processing treatments like stress relief can achieve predominantly fine grain structures under both conditions. To mitigate this issue, shot peening is employed, inducing compressive residual stress and promoting grain refinement, while reducing tensile residual stresses.

The stress-relieved honeycomb and gyroid metallic micro-lattice structures exhibit fine-grained compositions, enhancing their blast mitigation capabilities. These structures demonstrate notable strength and toughness, making them less susceptible to deformation and failure upon impact [18]. The presence of grain boundaries between adjoining cells contributes to improved mechanical properties, while gyroid structures' refined microstructure enhances their strength, stiffness, and fatigue resistance under impact loading [19]. To further optimize the material's properties, the test specimens undergo heat treatment.

Heat treatment enhances mechanical properties, including strength, hardness, and ductility, by refining the microstructure. In the SEM image

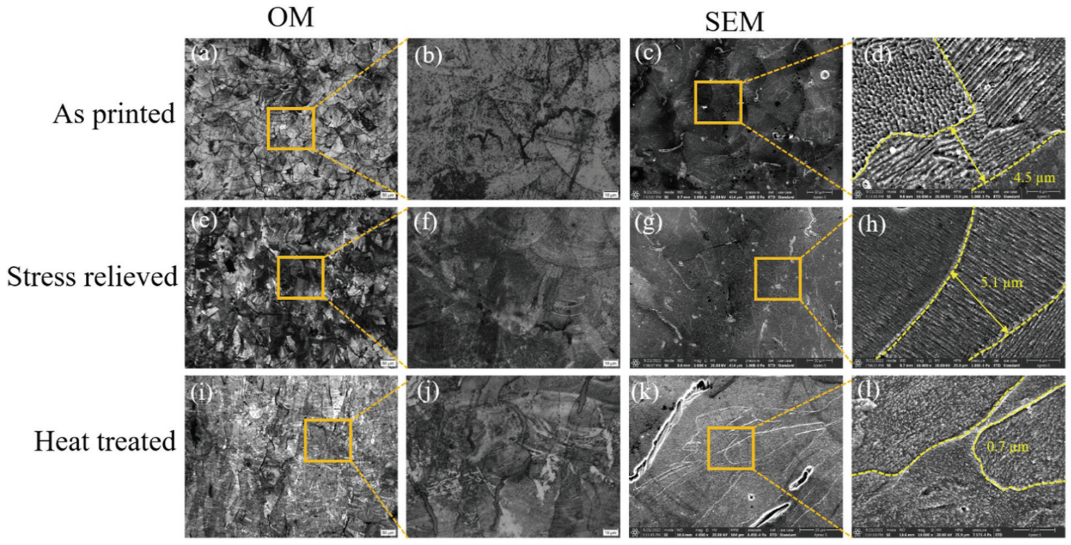


Fig. 6. OM and SEM images for honeycomb lattice structures: (a–d) as printed; (e–h) stress relieved; (i–l) heat treated

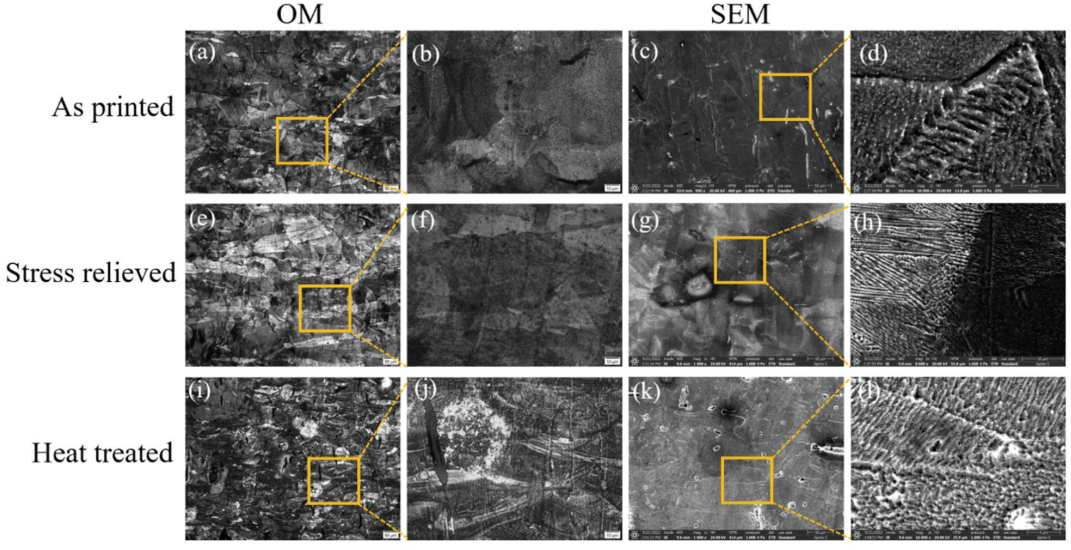


Fig. 7. OM and SEM images for gyroid lattice structures: (–d) as printed. (e–h) stress relieved, (i–l) heat treated

of honeycomb structures, distinct boundary lines indicate the presence of grain boundaries, reinforcing mechanical properties and blast mitigation capabilities. The refined gyroid structure exhibits increased strength, stiffness, and fatigue resistance under impact loading, although its SEM images lack well-defined boundaries due to its microstructural attributes. Overall, heat treatment effectively improves the microstructure of both structures, resulting in fine-grained materials with enhanced mechanical characteristics and blast mitigation capabilities, making honeycomb structures suitable for diverse applications, including blast mitigation [20].

3.3. Corrosion analysis

Corrosion analysis of honeycomb and gyroid micro-lattice structures is crucial for optimizing their blast mitigation effectiveness [21]. Corrosion can weaken metallic materials, compromising their



Fig. 8. Micro-lattice A286 test specimens placed in salt spray test chamber

Table 8. Corrosion rate for RHA, MHA, HNS, honeycomb, and gyroid micro-lattice structures

Case	Specimen	Initial weight (g)	Final weight (g)	Total weight loss (g)	Corrosion rate (mm/ year)
Existing materials	RHA	12.4093	12.4029	0.0064	2.847817577
	MHA	11.8837	11.8795	0.0042	1.868880285
	HNS	13.6118	13.6066	0.0052	2.313851781
Honeycomb lattice structure	5D (ideal)	77.6933	77.3803	0.313	1.218227858
	6D (non-ideal)	80.6307	80.3128	0.3179	1.237299156
Gyroid	1D	40.0436	39.9027	0.1409	1.671511872

Table 9. Corrosion rate for honeycomb and gyroid micro-lattice structures after compression test

Case	Specimen	Initial weight (g)	Final weight (g)	Total weight loss (g)	Corrosion rate (mm/year)
Honeycomb lattice structure	5C (ideal)	82.129	81.6725	0.4565	1.776744463
	6C (non-ideal)	78.4252	77.9683	0.4569	1.778301304
Gyroid	1C	32.1465	31.9494	0.1971	2.338218523

mechanical properties and reducing their ability to withstand blasts. Accelerated lab corrosion testing was performed using a salt spray chamber at a DRDO facility illustrated in Figure 8. Results for the corrosion rate are presented in Table 8, and the correlation between honeycomb, gyroid A286 micro-lattice structures, RHA, MHA, and HNS is shown in Table 9, providing valuable insights for enhancing their performance in blast mitigation applications.

Honeycomb and gyroid micro-lattice structures exhibit significantly lower corrosion rates compared to RHA, MHA, and HNS materials, as shown in Table 10. The corrosion resistance attenuation for honeycomb and gyroid A286 micro-lattice structures in correlation to RHA, MHA, and HNS before compression tests is 57.23%, 34.83%, 47.36%, and 41.31%, 10.6%, 27.75%, respectively. After compression tests, the attenuation in corrosion resistance is 37.61%, 4.92%, 23.21% for honeycomb and 17.88%, 25.16%, 1.08% for gyroid in correlation to RHA, MHA, and HNS, respectively. The higher surface area-to-volume ratio of honeycomb and gyroid

Table 10. Corrosion resistance (in %) of micro-metallic lattice structures: honeycomb and gyroid vs. RHA, MHA, and HNS

Before compression			
Comparison of corrosion rate	**Percentage difference**	**Comparison of corrosion rate**	**Percentage difference**
Honeycomb vs. RHA	57.23%	Gyroid vs. RHA	41.31%
Honeycomb vs. MHA	34.83%	Gyroid vs. MHA	10.6%
Honeycomb vs. HNS	47.36 %	Gyroid vs. HNS	27.75%
After compression tests			
Honeycomb vs. RHA	37.61%	Gyroid vs. RHA	17.88%
Honeycomb vs. MHA	4.92%	Gyroid vs. MHA	25.16%
Honeycomb vs. HNS	23.21%	Gyroid vs. HNS	1.08%
Micro-metallic lattice structures			
Honeycomb vs. gyroid (before compression)		27.11%	
Honeycomb vs. gyroid (after compression)		24.03%	

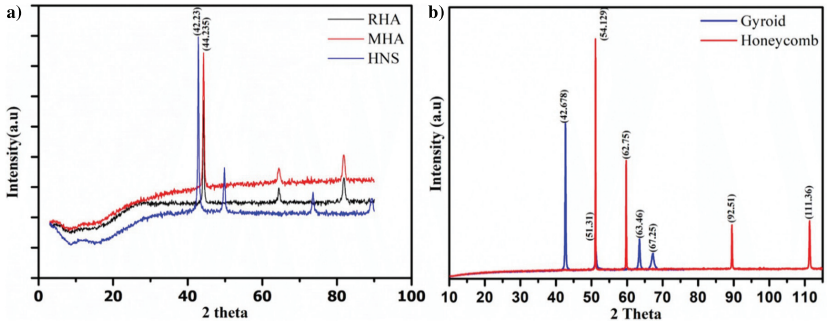


Fig. 9. X-ray diffraction plot (a) RHA, MHA, HNS; (b) honeycomb and gyroid micro-lattice structures

Table 11. Compressive residual stress for RHA, MHA, HNS, honeycomb and gyroid micro-lattice structures

Material	**Compressive residual stress values (MPa)**
Existing Materials	
RHA	306.627
MHA	348.454
HNS	432.367
Micro-metallic lattice structures	
Honeycomb	581.907
Gyroid	483.679

micro-lattice structures, along with their unique interconnected cellular geometry, contributes to their superior corrosion resistance and enhanced durability.

The interconnected cellular configuration of the honeycomb micro-lattice ensures a homogeneous stress distribution, reducing localized stress concentrations that can trigger corrosion. This feature mitigates the risk of localized corrosion and material deterioration. Additionally, the expanded surface area and distinctive microstructure contribute to its superior corrosion resistance compared to the gyroid micro-lattice. The innate robustness and rigidity of honeycomb and gyroid micro-lattice structures make them highly effective in blast mitigation, with a longer lifecycle compared to traditional materials. In contrast, conventional materials like RHA, MHA, and HNS display higher corrosion rates, compromising their mechanical properties and resilience, making them less reliable for blast mitigation applications, especially in underbody AFV use across different terrains.

3.4. Residual stress analysis – XRD

Residual stress analysis is crucial for enhancing blast mitigation in armoured fighting vehicles,

Table 12. Compressive residual stress comparison of micro metallic lattice structures honeycomb and gyroid vs. RHA, MHA, and HNS

Comparison of residual stress values	**% Increase in residual stress**	**Comparison of residual stress values**	**% Increase in residual stress**
Honeycomb vs. RHA	47.30%	Gyroid vs. RHA	36.6%
Honeycomb vs. MHA	40.12%	Gyroid vs. MHA	27.96%
Honeycomb vs. HNS	25.70%	Gyroid vs. HNS	10.61%
Micro-metallic lattice structures			
Honeycomb vs. Gyroid		16.88%	

particularly in the underbody region. It provides insights for armour design improvement, identifies vulnerable areas for strategic reinforcement, and aids in refining manufacturing processes [22, 23]. The central XRD facility offers residual stress data for A286 honeycomb and gyroid micro-lattice structures in correlation with RHA, MHA, and HNS materials, as depicted in Figure 9 and Table 11.

Table 11 reveals a distinct contrast in residual stress measurements between micro-lattice structures and conventional monolithic materials. Table 12 reveals that the compressive residual stress attenuation in honeycomb A286 micro-metallic lattice structures is 47.30%, 40.12%, and 25.70% in relation to RHA, MHA, and HNS material, respectively. The study reveals that gyroid A286 micro-metallic lattice structures exhibit attenuation percentages of 36.6%, 27.96%, and 10.61% in relation to RHA, MHA, and HNS materials, respectively. In relation to micro-lattice structures such as honeycomb and gyroid, it has been observed that the compressive residual stress attenuation is 16.88% higher in honeycomb as compared to the gyroid lattice structure.

Metallic micro-lattice structures, particularly honeycomb ones, exhibit high compressive residual stress, making them promising for blast mitigation (16.88% attenuation compared to gyroid lattice). During a blast event, the lattice structure efficiently absorbs and disperses the energy of the blast wave while maintaining its structural integrity, preventing catastrophic failure. In contrast, conventional materials like RHA, MHA, and HNS lack equivalent compressive residual stress and are susceptible to brittle fracture under blast-loading circumstances. The distinctive geometry of honeycomb micro-lattice structures with interconnected hexagonal cells generates high compressive residual stress, enhancing endurance against fatigue and crack propagation. On the other hand, gyroid lattice structures, with a recurring cubic unit cell, possess favourable mechanical properties but lack comparable compressive residual stress as honeycomb structures [6]. In a blast event, the honeycomb micro-lattice structure undergoes controlled deformation, efficiently absorbing and redistributing the blast wave's energy, preserving structural integrity, and avoiding catastrophic failure due to elevated compressive residual stress [7]. Gyroid lattice structures may lack equivalent compressive residual stress, making them susceptible to brittle fracture under blast-loading conditions [8]. In comparison, honeycomb structures exhibit significant strength, making them more suitable for blast mitigation applications.

4. Conclusions

Because of the nature of RHA, MHA, and HNS as monolithic materials, their non-availability in powder form restricts the formation of novel designs or adaptation to lattice designs in conventional or additive manufacturing processes. Modular structures are developed for the same purpose by adapting the LPBF process for additive manufacturing of A286 honeycomb and gyroid micro-lattice structures, which have demonstrated superior blast mitigation capabilities in comparison to conventional materials, which are highlighted to support an additional alternative for AFV application as follows:

1. This study focuses on developing micro-lattice structures using A286 steel through the LPBF process, adhering to industry standards. The A286 steel powder contains multiple elements that synergistically enhance blast mitigation properties, including thermal stability and durability. Microscopic examination showed spherical-shaped powders and improved mechanical attributes and surface texture during fabrication. The research analyses LPBF A286 honeycomb and gyroid structures, considering surface roughness and micro-Vickers hardness for non-stress-relieved, stress-relieved, and heat-treated specimens. The aim is to gain a comprehensive understanding of the armour's efficacy in defending against explosive attacks.
2. The TOPSIS method was used to find close-to-ideal dimensions for honeycomb A286 micro-lattice structures under different conditions. For non-stress-relieved and stress-relieved specimens, the dimensions are $24 \times 20 \times 30\,mm^3$ (L × W × H) with a wall thickness of 2 mm, hole diameter of 0.8 mm, and infill thickness of 0.8 mm. For heat-treated (final) specimens, the dimensions are the same except for a hole diameter of 1 mm and infill thickness of 1 mm by taking response attributes as surface roughness and micro-Vickers hardness in correlation to design lattice.
3. Surface morphology analysis of post-processed micro-lattice honeycomb and gyroid specimens reveals fine grains and reduced grain boundary thickness. The micro-lattice structures exhibit optimized grain structure and induced residual stresses, leading to attenuation of material strength, ductility, and fatigue resistance. This internal mechanism mitigates the propagation of cracks and defects during blast events.
4. Micro-lattice honeycomb structures show improved strength and toughness due to reduced and uniformly refined grain boundaries acting as dislocation barriers. Gyroid micro-lattice structures exhibit greater refinement, enhancing strength, stiffness, and fatigue resistance under impact loading. Lack of well-defined boundaries in AFVs is attributed to microstructural properties, not subpar mechanical attributes, highlighting their potential for blast mitigation.
5. Honeycomb and gyroid micro-lattice structures offer superior corrosion resistance compared to RHA, MHA, and HNS. Before compression tests, honeycomb structures show attenuation of corrosion resistance by 57.23%, 34.83%, and 47.36%, while gyroid structures show 41.31%, 10.6%, and 27.75%. After compression tests, attenuation for honeycomb structures is 37.61%, 4.92%, and 23.21%, and for gyroid structures it is 17.88%, 25.16%, and 1.08%.
6. Honeycomb and gyroid micro-lattice structures offer superior corrosion resistance and durability compared to conventional materials. Their unique geometry, expanded surface area, and enhanced stress distribution contribute to their effectiveness in blast mitigation. They are reliable options for long-term protection against corrosion and blast-induced damage in diverse AFV terrains.
7. The honeycomb A286 micro-metallic lattice structures experience a 47.30%, 40.12%, and 25.70% attrition in compressive residual stress compared to RHA, MHA, and HNS materials, respectively. For gyroid A286 micro-metallic lattice structures, the attenuations are 36.6%, 27.96%, and 10.61% compared to RHA, MHA, and HNS materials, respectively. The unique geometry of honeycomb structures, with slender walls undergoing bending and buckling, contributes to the stress attenuation. Gyroid lattice structures exhibit higher resistance to brittle fracture, making them promising for blast mitigation, despite lower residual stress levels.

Metallic 3D printing technology shows great potential for creating micro-lattice materials, opening new possibilities for scientific and technological advancements. These materials can find applications beyond AFVs and blast mitigation. The unique geometry of lattice structures affects their mechanical properties, with thin walls undergoing bending and buckling during loading and unloading, leading to stress redistribution. The honeycomb lattice's resistance to brittle fracture makes it promising for blast mitigation.

Symbols

S_i^+ **:** Distance of x_i from ideal solution
S_i^- **:** Distance of x_i from negative ideal solution
C_i **:** Relative closeness of x_i to ideal solution
R_a **:** Surface mean roughness

Abbreviations and acronyms

AFV	: armoured fighting vehicle
LPBF	: laser powder bed fusion
RHA	: rolled homogeneous armour
MHA	: mild homogeneous armour
HNS	: high-nitrogen steel
MCDM	: multi-criteria decision-making
TOPSIS	: technique for order of preference by similarity to ideal solution
EDM	: electrical discharge machining
FEA	: finite element analysis
XRD	: X-ray diffraction
SEM	: scanning electron microscopy

Labels, units, and organizational acronyms

A286	: A type of steel
MFT-5000	: Tribometer model
DRDO	: Defence Research and Development Organisation
CVRDE	: Combat Vehicles Research Establishment
DMRL	: Defence Metallurgical Research Laboratory
MPa	: megapascals
$^\circ$ C	: degrees celsius
μm	: micrometers
s	: seconds
Gwyddion	: software for data post-processing

Acknowledgements

The Principal Investigator, Dr. C. Chandrasekhara Sastry and fellow authors thank ARMREB (Armaments Research Board), DRDO (Defence Research Development Organisation), defence labs CVRDE (Combat Vehicles Research Establishment) and DMRL (Defence Metallurgical Research Laboratory), for providing funding and resources for the completion of the defence work, which is reported here. The authors are also grateful to DRDO for providing requisite facilities to perform the experiments and further analysis.

References

[1] Ashby MF, Gibson LJ. *Cellular solids: structure and properties*. Cambridge (UK): Press Syndicate of the University of Cambridge; 1997. p. 175–231.

[2] Wang Z. Recent advances in novel metallic honeycomb structure. *Compos. B. Eng.* 2019;166:731–41. doi: 10.1016/j.compositesb.2019.02.011

[3] Germscheidt RL, Silva MB, Datti E, Bonacin JA. Materials and challenges of 3D printing for defense applications and humanitarian actions. In: Gupta RK, editor. *3D printing: fundamentals to emerging applications*. Boca Raton (FL): CRC Press; 2023. p. 471–83.

[4] Deters J. 3D printing impacts on systems engineering in the defense industry. In: Badiru AB, Valencia VV, Liu D, editors. *Additive manufacturing handbook*. Boca Raton (FL): CRC Press; 2017. p. 49–56.

[5] Zhang S, Chen W, Gao D, Xiao L, Han L. Experimental study on dynamic compression mechanical properties of aluminium honeycomb structures. *Appl. Sci*. 2020;10(3):1188. doi: 10.3390/app10031188

[6] Thirumavalavan K, Chandrasekhar SC, Abeens M, Muruganandhan R, Manickam MM. Study on the influence of process parameters of severe surface mechanical treatment process on the surface properties of AA7075 T651 using TOPSIS and Taguchi analysis. *Mater Res Express*. 2019;6(11):1165i1. doi: 10.1088/2053-1591/ab522f

[7] Sastry CC, Abeens M, Pradeep N, Manickam MM. Microstructural analysis, radiography, tool wear characterization, induced residual stress and corrosion behavior of conventional and cryogenic trepanning of DSS 2507. *J Mech Sci Technol*. 2020;34:2535–47. doi: 10.1007/s12206-020-0529-1

[8] Pradeep N, Shaik AM, Rahman HA. Patil S. Experimental investigation of electrodeposited Ni-Al2O3/ZrO2 nano composite on HSLA ASTM A860 alloy. *Surf Topogr Metrol Prop*. 2021;9(4):045028. doi: 10.1088/2051-672X/ac396a

[9] Li T, Wang L. Bending behavior of sandwich composite structures with tunable 3D-printed core materials. *Compos Struct*. 2017;175:46–57. doi: 10.1016/j.compstruct.2017.05.001

[10] Bogusz P, Popławski A, Stankiewicz M, Kowalski B. Experimental research of selected lattice structures developed with 3D printing technology. *Materials*. 2022;15(1):378. doi: 10.3390/ma15010378

[11] Butt MZ, Ali D, Aftab M, Bashir F, Pervaiz MS, Tanveer MU, Khaliq MW. Nitrogen ions implantation in W-based quad alloy: structure, electrical resistivity, surface roughness and Vickers hardness as a function of ion dose. *Met Mater Int*. 2021;27:3342–58. doi: 10.1007/s12540-020-00861-z

[12] Sastry CC, Hariharan P, Pradeep Kumar M, Muthu Manickam MA. Experimental investigation on boring of HSLA ASTM A36 steel under dry, wet, and cryogenic environments. *Mat Manufact Proc*. 2019;34(12): 1352–79. doi: 10.1080/10426914.2019.1643477

[13] Alizadeh-Sh M, Marashi SPH, Ranjbarnodeh E, Shoja-Razavi R, Oliveira JP. Dissimilar laser cladding of Inconel 718 powder on A-286 substrate: microstructural evolution. *J Laser Appl*. 2020;32(2). doi: 10.2351/1.5124932

[14] Hazell PJ. *Armour: materials, theory, and design*. 1st ed. Boca Raton (FL): CRC Press; 2015. P. 182–274. ebook ISBN 978042915660

[15] Dong FY, Zhang P, Pang JC, Ren YB, Yang K, Zhang ZF. Strength, damage and fracture behaviors of high-nitrogen austenitic stainless steel processed by high-pressure torsion. *Scr Mater*. 2015;96, 5–8. doi: 10.1016/j.scriptamat.2014.09.016

[16] Qi C, Yang S, Yang LJ, Wei ZY, Lu ZH. Blast resistance and multi-objective optimization of aluminum foam-cored sandwich panels. *Compos Struct*. 2013;105:45–57. doi: 10.1016/j.compstruct.2013.04.043

[17] Dharmasena KP, Wadley HN, Xue Z, Hutchinson JW. Mechanical response of metallic honeycomb sandwich panel structures to high-intensity dynamic loading. *Int J Impact Eng*. 2013;35(9):1063–74. doi: 10.1016/j.ijimpeng.2007.06.008

[18] Evans AG, He M, Deshpande VS, Hutchinson JW, Jacobsen AJ, Carter WB. Concepts for enhanced energy absorption using hollow micro-lattices. *Int J Impact Eng*. 2010;37(9):947–59. doi: 10.1016/j.ijimpeng.2010.03.007

[19] Davami K, Mohsenizadeh M, Munther M, Palma T, Beheshti A, Momeni K. Dynamic energy absorption characteristics of additively manufactured shape-recovering lattice structures. *Mater Res Express*. 2019;6(4):045302. doi.org/10.1088/2053-1591/aaf78c

[20] Li D, Qin R, Xu J, Chen B, Niu X. Effect of heat treatment on AlSi10Mg lattice structure manufactured by selective laser melting: microstructure evolution and compression properties. *Mater Charact*. 2022;187:111882. doi: 10.1016/j.matchar.2022.111882

[21] Khan HM, Özer G, Yilmaz MS, Koç E. Corrosion of additively manufactured metallic components: a review. *Arab J Sci Eng*. 2022;47(5):5465–90. doi: 10.1007/s13369-021-06481-y

[22] Ahmed N, Barsoum I, Abu Al-Rub RK. Numerical investigation on the effect of residual stresses on the effective mechanical properties of 3D-printed TPMS lattices. *Metals*. 2022;12(8):1344. doi: 10.3390/met12081344

[23] Kelin LI, Yangjilian LIAO, Lin GU, Guojian HE, Wansheng ZHAO. Study on residual stress of blasting erosion arc machined Ti6Al4V and TiAl alloys. *Proc CIRP*. 2022;113:507–12. doi: 10.1016/j.procir.2022.09.168

Received 2023-08-04
Accepted 2023-09-13